1-1-2013

Rational design of p-type thermoelectric PbTe: Temperature dependent sodium solubility

Sima Aminorroaya-Yamini
University of Wollongong, sima@uow.edu.au

Teruyuki Ikeda
California Institute of Technology

Aaron Lalonde
California Institute of Technology

Yanzhong Pei
California Institute of Technology

S X. Dou
University of Wollongong, shi@uow.edu.au

See next page for additional authors

Rational design of p-type thermoelectric PbTe: Temperature dependent sodium solubility

Abstract

We develop a solid understanding of the termperature-dependent solubility of sodium p-type PbTe, the most efficient thermoelectric material. The maximum solubility of socium telluride (NaTe) in PbTe is measured to be 1.4+0.3 at percent and the heat of solution is evaluated and that addresses fundamental issues regarding the formation of nano-precipitates.

Keywords

thermoelectric, pbte, temperature, dependent, sodium, rational, solubility, design, p, type

Disciplines

Engineering | Physical Sciences and Mathematics

Publication Details

Aminorroaya Yamini, S., Ikeda, T., Lalonde, A., Pei, Y., Dou, S. Xue. & Snyder, G. Jeffrey. (2013). Rational design of p-type thermoelectric PbTe: Temperature dependent sodium solubility. Journal of Materials Chemistry A, 1 (31), 8725-8730.

Authors

Sima Aminorroaya-Yamini, Teruyuki Ikeda, Aaron Lalonde, Yanzhong Pei, S X. Dou, and G. Jeffrey Snyder

Journal of Materials Chemistry A

RSC Publishing

COMMUNICATION

View Article Online
View Journal | View Issue

Cite this: J. Mater. Chem. A, 2013, 1, 8725

Received 26th April 2013
Accepted 20th June 2013

DOI: 10.1039/c3ta11654a

www.rsc.org/MaterialsA

Rational design of p-type thermoelectric PbTe: temperature dependent sodium solubility

Sima Aminorroaya Yamini,*[a] Teruyuki Ikeda,[b] Aaron Lalonde,[b] Yanzhong Pei,[b] Shi Xue Dou[a] and G. Jeffrey Snyder*[b]

We develop a solid understanding of the temperature-dependent solubility of sodium in p-type PbTe, the most efficient thermoelectric material. The maximum solubility of sodium telluride (NaTe) in PbTe is measured to be 1.4 ± 0.3 at% and the heat of solution is evaluated as 26^{+19}_{-11} kJ mol^{-1} that addresses fundamental issues regarding the formation of nano-precipitates.

Thermoelectric energy converters are expected to play a significant role in clean and renewable energy, and to reduce the reliance on fossil fuelled heat engines that generate approximately 90% of the world's electrical power at a typical 30–40% efficiency. The maximum efficiency of thermoelectric materials is determined by the dimensionless figure of merit, $zT = S^2T\sigma/(\kappa_e + \kappa_L)$, which is a function of lattice thermal conductivity (κ_L), electronic thermal conductivity (κ_e), the Seebeck coefficient (S), electrical conductivity (σ), and absolute temperature.

Although a feasible thermoelectric generator for primary power generation requires thermoelectric materials with zT above 1.5 at 800 °C operation temperature,[1] the small size, rapid response and robustness of thermoelectric generators have made them rival candidates for several successful applications.[2] Recently, a large number of studies[3–7] have focused on the so-called mid-range temperature (600–900 K) thermoelectric materials, specifically Pb chalcogenides, where the majority of broad-based applications could benefit. PbTe is the premiere mid-range temperature thermoelectric material. Latest studies[3,4,7] have reported significant improvement of its thermoelectric performance through tuning of the electronic structure and/or the nanostructuring of bulk materials. Intrinsic semiconducting lead telluride can be tuned either to the n-type or p-type as it can contain as many as approximately 1.5×10^{18} electrons or 7.7×10^{18} holes per cm^3 due to excess lead or tellurium atoms respectively.[8] These point defects act as donors ($[V''_{Te}]$) or acceptors ($[V^{\cdot\cdot}_{Pb}]$). However, precise control of hole concentration in p-type PbTe (ranging from $\sim 10^{18}$ to $\sim 10^{20}$ cm^{-3}) has been achieved through substitution of monovalent atoms of thallium,[7] sodium[9,10] or potassium[11,12] on the lead sublattice. Alkali metals (Li, Na, K, Rb, Cs), Ag and Tl are likely candidates for p-type doping of PbTe. Nevertheless, atoms with an ionic radius larger than that of *K* cannot be efficiently doped due to steric interaction, and Tl alters the band structure with resonant states.[7] Interstitial Ag (ref. 13) can also act as an n-type dopant and Ag ionic conductivity in PbTe shows mobility.[14]

Although sodium has been the most viable dopant for PbTe,[9,15,16] its solubility level at various temperatures has not been studied systematically and little attention has been given to the relevant phase diagrams. The band structure of PbTe is typically considered rigid and it is believed that electronic transport properties of N-doped PbTe are affected by heavy effective mass holes, resulting from a high density of states (DOS) near the Fermi level.[17]

The only available pseudo-binary phase diagrams of PbTe–NaTe and PbTe–Na_2Te (ref. 18) do not determine the solubility of sodium in PbTe. It is generally believed that the Na solubility in PbTe is above 0.5% up to 1.75% although some loss of Na may occur during processing. The maximum carrier concentration, according to Hall effect measurements at 77 K, that is observed in Na-doped PbTe is 2.5×10^{20} cm^{-3} and it is believed that each Na atom donates about 1 hole when Na concentration is higher than $\sim 6 \times 10^{19}$ cm^{-3}, which corresponds to approximately $x = 0.017$ in $Na_xPb_{(1-x)}Te$.[10] In recent microscopic studies[14,19] on sodium doped (more than 1 at%) PbTe samples, nano-scale precipitates have been observed which are suggested to be sodium-rich lead telluride ($Na_xPb_{(1-x)}Te$) precipitates[14] distributed in a slightly doped (~0.5%) lead telluride matrix. However, the temperature history of the sample may play a significant role in the solubility of sodium as dopant solubility changes with temperature, as has been found in several PbTe pseudo-binary systems.[20,21]

[a]Australian Institute for Innovative Materials (AIIM), Innovation Campus, University of Wollongong, NSW 2519, Australia. E-mail: sima@uow.edu.au; Fax: +61 242215731; Tel: +61 242981401

[b]Materials Science, California Institute of Technology, Pasadena, CA 91125, USA. E-mail: jsnyder@caltech.edu; Tel: +1 6265026126

In this report, the lead telluride rich side of the PbTe–NaTe phase diagram is revisited to understand the sodium solubility in samples with various heat treatment histories. We measured the solubility of sodium in PbTe by Wavelength Dispersive Spectroscopy (WDS) in an Electron Probe Micro-Analyser (EPMA) at various annealing temperatures. Furthermore, the maximum solubility of sodium in PbTe has been determined. The heat of solution of precipitates in the solid PbTe matrix is calculated and the effect of sodium addition on the nature and formation of nano-precipitates and the microstructure of polycrystalline $Na_xPb_{(1-x)}Te$ are discussed.

Polycrystalline $Na_xPb_{(1-x)}Te$ ($x = 0.02$, 0.05) samples were synthesized by mixing appropriate amounts of high purity Pb (99.999%), Te (99.9999%) and Na (99%), with a total mass of 10 g, sealed in carbon-coated quartz tubes under vacuum and heated to 1050 °C at ~100 °C h^{-1}. After holding at 1050 °C for about 6 hours, the ampoules were cold-water quenched and either annealed at 507 °C and 300 °C for a week or at 500 °C for 48 hours and then quenched in salt water (~−15 °C). The last ingot was ground into a powder and hot pressed in a 12 mm diameter graphite mould under an axial pressure of 40 MPa and argon atmosphere at 500 °C for 1 h. The pellet with a relative density of 98% or higher was used for simultaneous measurements of the resistivity and the Hall coefficient (R_H) using the van der Pauw technique under a reversible magnetic field of 2 T.[22]

Two hot-pressed $Na_{0.02}Pb_{0.98}Te$ samples were sealed in evacuated quartz tubes and heated to 800 °C for 8 hours and then annealed at that temperature for 6 hours. Then they were cooled to 350 °C and 240 °C by slow cooling at the rate of 10 °C h^{-1} to avoid the formation of a fine secondary phase due to the high degree of non-equilibrium and then annealed at that temperature for two days and three weeks respectively followed by quenching in iced salt water to provide the fastest quenching rate and avoid inner-grain precipitation.

The samples were examined by field emission gun-scanning electron microscopy (SEM), using a Carl Zeiss LEO 1550 VP equipped with an Energy Dispersive X-ray Spectrometer (EDS). Samples were subjected to chemical composition analysis by wavelength-dispersive X-ray spectrometry (WDS) using an electron probe X-ray MicroAnalyser (JXA-JEOL 8200). In the WDS measurements, the intensities of Te L_α, Pb M_α, and Na K_α were measured and corrected by the ZAF method to obtain chemical compositions. PbS, Te and Albite ($NaAlSi_3O_8$) standards were used for the ZAF corrections of Te, Pb and Na respectively. The EPMA was operated under a 15 kV accelerating voltage and 25 nA probe current. For regions containing precipitates, the smallest probe diameter was set to measure the matrix compositions.

The optimum p-type carrier concentration in PbTe-based alloys has been achieved at ~10^{20} cm^{-3} with the addition of approximately 1 at% Na ($Na_{0.02}Pb_{0.98}Te$).[9,15,23] Therefore, in the current study a sample with a nominal composition of $Na_{0.02}Pb_{0.98}Te$ (1 at% Na) was prepared by quenching the equilibrated liquid at 1050 °C and annealing at 300 °C for 5 days followed by quenching in cold water. The scanning electron microscopy (SEM) image of the polished annealed sample in Fig. 1(a) clearly illustrates the presence of precipitates (up to 500 nm). Energy Dispersive Spectroscopy (EDS) analysis of precipitates indicates the sodium rich phase. However, the accurate chemical composition of the precipitates cannot be determined due to the large interaction volume of the electron beam with the matrix compared to the precipitate size and the possible oxidation of precipitates whilst it undoubtedly shows that the 1 at% Na is not completely dissolved in the PbTe matrix at 300 °C. Another sample with the same composition ($Na_{0.02}Pb_{0.98}Te$) was annealed at 500 °C for two days, and then ground and hot pressed at the same temperature for an hour. While precipitates are not found in the matrix of the 500 °C annealed sample, Fig. 1(b) shows features at the junction between particles (grain boundaries), where the sintering occurred. The round features on the surface that contain reaction products (Fig. 1(b) inset) suggest the presence of a phase transformation that involves a liquid phase. EDS analysis of these features indicates the presence of sodium and proves the diffusion of sodium to grain boundaries and the formation of a liquid phase in equilibrium with lead telluride at the sintering temperature as suggested by the binary phase diagram of PbTe–NaTe. It is evident that the 1 at% Na is not completely dissolved at 500 °C.

The Hall coefficient (R_H) of the sintered sample was measured using the van der Pauw technique whereas the expected carrier concentration for complete solubility of 1 at% Na in PbTe is equal to 3.0×10^{20} based on the assumption that every lead atom which is replaced by sodium donates one hole to the final compound. It should be noted that the Hall concentration of electrical carriers (p) is determined from the Hall coefficient (R_H) assuming $p = 1/R_H$. It is generally understood that lead telluride has two valence bands (a light valence band at L points and a heavy band at $\sum$ points) which converge at approximately 430 K in highly doped samples[3,24,25] resulting in the maximum Hall coefficient value at that temperature. Therefore, the room temperature (~300 K) carrier concentration is smaller than the actual values and careful measurement of the carrier concentration for p-type PbTe should be performed at temperatures less than 100 K. The carrier concentration value in this study is reported only for the purpose of comparison to previous studies[9,10,14] on Na-doped PbTe.

In order to describe sodium doping in PbTe and gain insight into the nature and composition of the observed precipitates, it is required to know the ternary Na–Pb–Te system, specifically the phase equilibria of the PbTe–NaTe system as shown in Fig. 2(a) (adopted from ref. 18). The phase diagram shows no solubility of NaTe in PbTe although there have been some studies[10,19,26] showing solubility. Differential scanning calorimetry (DSC) and X-ray diffraction analysis techniques were employed by Finogenova *et al.*[18] to investigate the isoplethal PbTe–NaTe section, although these methods are not ideal for measuring solid solubility. Nevertheless, the complicated liquidus of the NaTe rich side of the phase diagram was fully investigated (Fig. 2(b)) and shows a eutectic transformation ($L = L' + Na_2Te + PbTe$) at 370 °C followed by a peritectic isotherm ($L_3 + Na_2Te = NaTe$) at 320 °C. It is anticipated that the maximum solubility of NaTe in PbTe occurs near these transformation temperatures (temperature range of 320–370 °C).

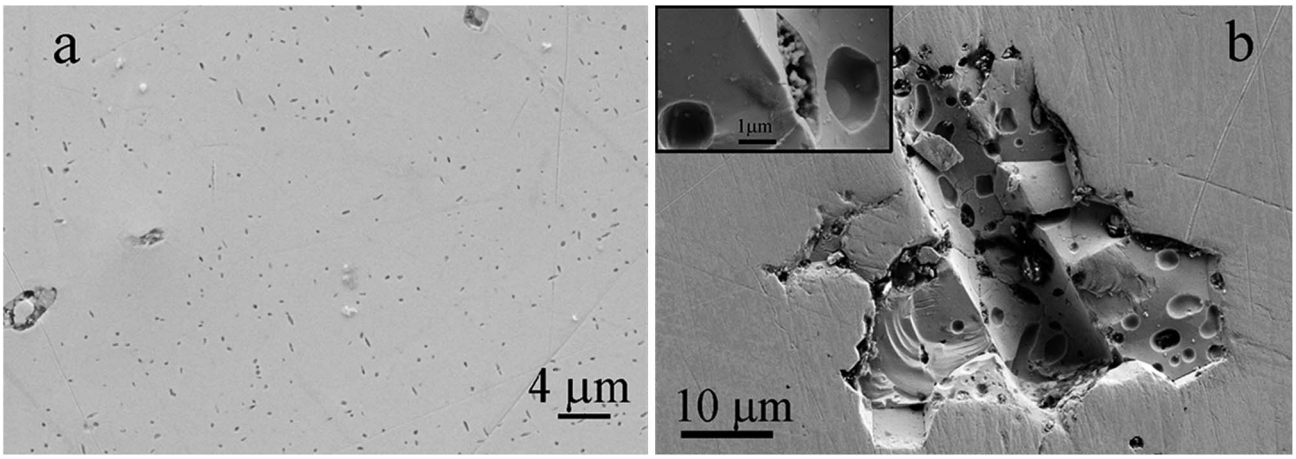

Fig. 1 SEM micrographs of (a) cast $Na_{0.02}Pb_{0.98}Te$ alloy which was quenched from the equilibrated melt and annealed at 300 °C for a week, (b) sintered $Na_{0.02}Pb_{0.98}Te$ alloy which was quenched from the equilibrated melt, annealed and sintered at 500 °C. The round features on the surface and reaction products suggest the presence of a liquid phase at the sintering temperature.

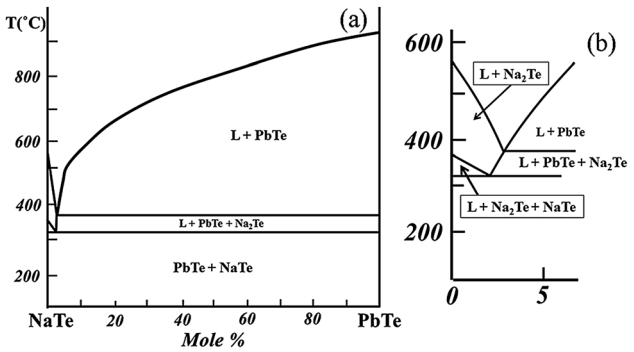

Fig. 2 (a) Temperature–composition projection of PbTe–NaTe cross-section of the Na–Pb–Te system, showing no solubility of NaTe in PbTe (adapted from (ref. 18)). (b) The NaTe rich side of the phase diagram is shown in more detail.

In the following section, sodium diffusion in PbTe will be reviewed to elucidate the mechanisms observed in this study. The diffusion coefficient of sodium at $\sim 10^{18}$ to 10^{19} cm^{-3} carrier concentration in a single crystal p-type PbTe follows eqn (1):[27]

$$D = 0.17\exp(-1.91/kT) \quad (1)$$

where D is the diffusion coefficient (cm^2 s^{-1}), k is Boltzmann's constant (in eV K^{-1}) and T is the absolute temperature (K). The diffusion coefficient is approximately 20 times faster at a higher carrier concentration (in a single crystal). Moreover, diffusion in polycrystalline samples, which is influenced by diffusion along grain boundaries (D_b) in addition to volume diffusion (D_v) is equal to:[25]

$$D_{eff} = \frac{D_v n_v + D_b n_b}{n_v + n_b} \quad (2)$$

where n_v and n_b are the concentrations of diffusing impurities on grain boundaries and in the interior of the crystal respectively. It is generally agreed that at temperatures $T > (0.8\text{–}0.9)T_m$, $D_v > D_b$ while at temperatures $T < (0.4\text{–}0.5)T_m$, $D_v < D_b$,[25] where T_m is the melting temperature of the matrix. Therefore, at high temperatures (over 0.8 T_m), diffusion within grains is dominant which results in a large diffusion distance and accelerates the phase separation reflecting the equilibrium phase boundary composition and giving a coarse microstructure. Consequently, we chose a temperature of 800 °C (~0.86 T_m) for the annealing of the sample to promote the diffusion within grains which could result in a coarse microstructure.

The fractured surface of the sample after heat treatment was studied by SEM and EDS analysis prior to chemical composition analysis by WDS as shown in Fig. 3. It is evident that sodium-rich particles which are expected to be the sodium telluride phase form on grain boundaries, as shown in Fig. 3(b) where the X-ray map illustrates sodium and tellurium at a grain boundary. This means that the NaTe concentration in $Na_{0.02}Pb_{0.98}Te$ surpasses the solubility of PbTe at 350 °C. Sodium telluride compounds are air-sensitive and oxidize initially to polytellurides, and finally to metallic Te and sodium oxide residue.

The samples annealed at 240, 350 and 507 °C were subjected to chemical composition analysis by WDS using an EPMA in order to carefully measure the sodium content in the matrix. The EPMA was operated under a 15 kV accelerating voltage. The excitation depth is expected to be around or less than 1 μm, which is smaller than the spacing between secondary phases, and therefore, the values measured for the lead telluride matrix are precise representatives of the equilibrium phase boundaries at the respective temperatures. The reported values are average values from more than 100 point analysis which was performed close to precipitates within the diffusion distance of sodium in lead telluride.

We have measured the solubility of Na at 240 °C to be approximately 0.24 ± 0.14 at%, which is equal to 0.48 mole percent NaTe in PbTe. Although the measurement error is higher at a low concentration of sodium in the matrix, the sodium shows considerable reduction in its solubility over 100 K temperature reductions. The measured values at 240 °C, 350 °C and 507 °C are presented in Fig. 4. Therefore, we suggest that the solubility of NaTe in PbTe at 350 °C, which is

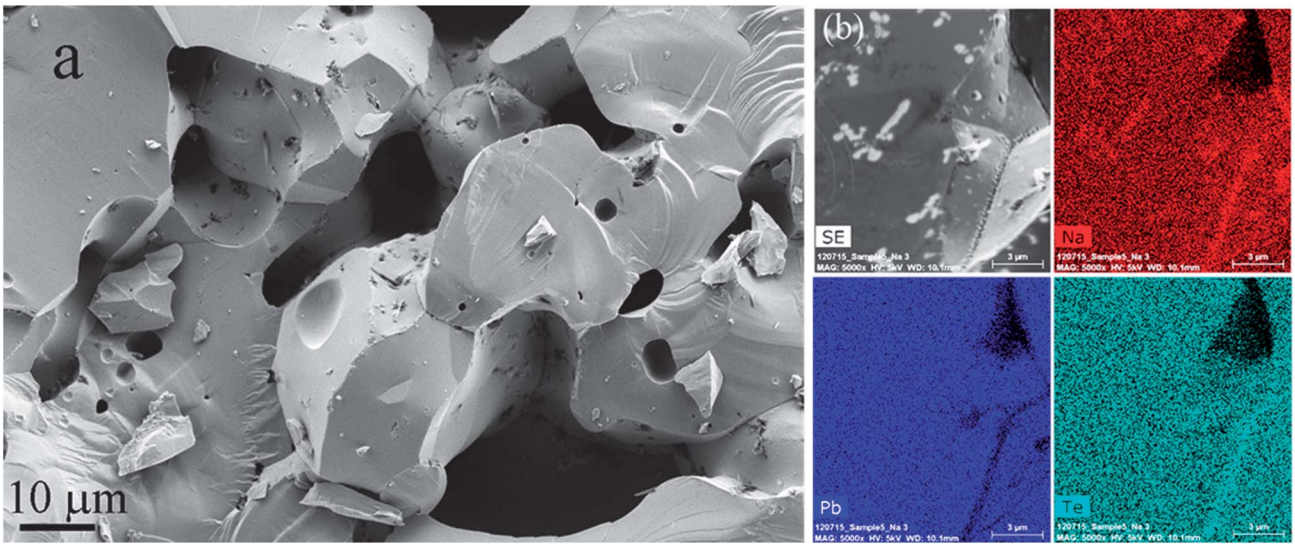

Fig. 3 (a) SEM micrographs of a fracture surface of the heat-treated sintered $Na_{0.02}Pb_{0.98}Te$ sample which was heated to 800 °C in 8 hours, annealed for 6 hours and cooled to 350 °C at 10 °C h^{-1}, followed by annealing at that temperature for two days and quenching in iced salt water, (b) EDS mapping of an area containing a grain boundary, showing particles rich in sodium and tellurium at the grain boundary.

anticipated to be close to the maximum solubility, for $Na_xPb_{(1-x)}Te$ is $x = 0.014 \pm 0.003$.

Crocker[10] attempted to measure the solubility of sodium in a sliced single crystal of sodium doped PbTe and reported a maximum of 2.5×10^{20} Na atoms per cm^3 which correspond to $x = 0.017$ in the $Na_xPb_{(1-x)}Te$ alloy. This conclusion was drawn from a graph in which sodium concentration *versus* the Hall carrier concentration at 77 K was plotted. At sodium concentrations above 2.5×10^{20}, the measured Hall carrier concentrations were scattered and remain almost constant. Therefore, this value was considered as the maximum sodium solubility. However, there are no experimental data available between approximately 7×10^{19} and 2.5×10^{20} per cm^3 sodium concentration. Moreover, the electrical carrier concentration was determined *via* $p = 1/(eR_H)$ while the Hall coefficient is related to the carrier concentration through the Hall factor, r_H, in the relationship $p = r_H/(eR_H)$ which has strong dependence on the doping level.[31] Although further investigation is required to explore the relationship between the sodium concentration and the carrier concentration, it is evident that this graph cannot be employed to determine the maximum sodium solubility. The recent high resolution transmission electron microscopy (TEM)[14] and atom probe tomography (APT)[19] analyses on similar samples indicate approximately 0.5 at% sodium solubility in the PbTe matrix which is consistent with the current study findings below 300 °C.

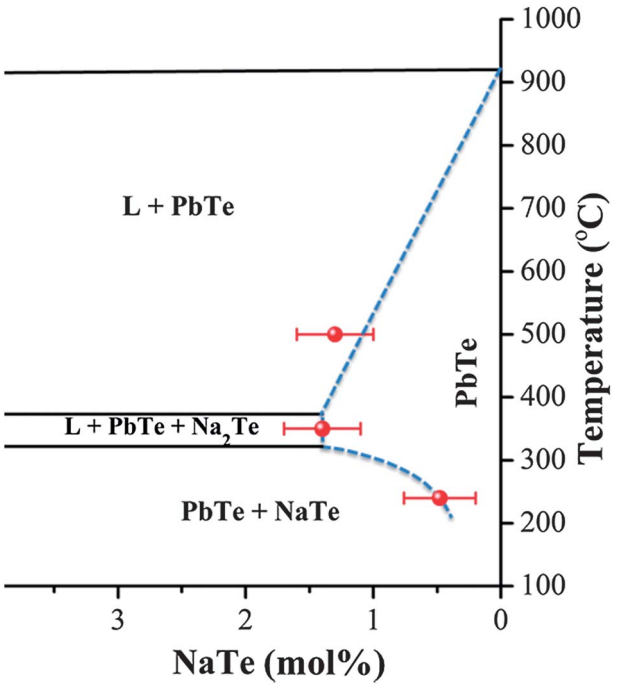

Fig. 4 Temperature–composition projection of PbTe–NaTe cross-section of the Na–Pb–Te system, showing the solubility of NaTe in PbTe.

The maximum solubility of NaTe in PbTe, ~0.7 at% Na, is smaller, compared to similar systems of PbTe–Sb_2Te_3 (6 at% Sb)[29] or PbTe–Ag_2Te (15 at% Ag).[28] The solubility of sodium in the lead telluride matrix is reduced significantly upon reducing the temperature below 320 °C, resulting in precipitation of NaTe when the sample is annealed at low temperatures (as shown in Fig. 1) or with continuous cooling of solid solution samples to room temperature.[14,19] In the following section, the relationship between the thermodynamic properties, solubility and precipitate size will be briefly discussed.

Isoplethal sections of the phase diagrams of PbTe–NaTe, PbTe–Ag_2Te and PbTe–Sb_2Te_3 reveal markedly low solubility of NaTe, very limited solubility of Ag_2Te and comparatively larger solubility of Sb_2Te_3 in the PbTe matrix. Here, we try to explain this fact by reviewing the Hume-Rothery rules[32] that introduce similarity in the atomic radius of the solute to that of the solvent atoms, similar valence and electronegativity and matching crystal structure to identify the degree of dissolution in solid

solution alloys of substitutional elements. The ionic radii of Ag^+ (0.115 nm) and Na^+ (0.102 nm) are comparable with the ionic radius of Pb^{2+} (0.119 nm), while they are considerably larger than that of Sb^{3+} (0.076 nm).[33] Therefore, atomic strain cannot be responsible for the poor solubility of Ag^+ and Na^+ in the PbTe matrix. However, the electronegativity of Pb, Te, Sb, Ag and Na is equal to 3.08, 3.59, 3.34, 2.59, and 0.70, respectively, by Sanderson's definition.[34] The difference in electronegativity of the anion, Te, from that of the cations in the matrix phase is more pronounced in the case of Ag and Na than that of Sb, indicating greater attraction of Ag and Na atoms for bonding electrons of telluride in the chemical bonds compared with Pb and Sb. Moreover, NaTe crystallizes in the orthorhombic structure[35] and Ag_2Te in the monoclinic while Sb_2Te_3 has a hexagonal structure that is more similar to the FCC structure of the lead telluride matrix.

Nucleation of precipitates in the matrix remains to be assessed. The driving force of precipitate nucleation (ΔG_{chem}) is proportional to the heat of solution as[36]

$$\Delta G_{chem} = -\Delta H_s \frac{\Delta T}{T_s} \quad (3)$$

where ΔH_s is the heat of solution, ΔT is the degree of supercooling, and T_s is the solvus temperature. Thus, in general, the larger the heat of solution, the higher is the chemical driving force, which leads to a higher nucleation rate and hence a finer precipitate microstructure.

For a dilute solution in a eutectic binary system consisting of elements A and B where A and B form α and β phases, respectively, with different crystal structures, B is soluble in the α phase, and the solubility of A in the β phase is negligible; the solubility of B in the α phase x_B^α is expressed as:

$$x_B^\alpha = A\exp\left(-\frac{\Delta H_s}{RT}\right) \quad (4)$$

where A is a constant, ΔH_s is the heat of solution, R is the gas constant, and T is the absolute temperature.[37] Fig. 5 shows the temperature dependent solubility of NaTe in PbTe compared with those of Ag_2Te (ref. 28) and Sb_2Te_3.[29] Here, the atomic fractions of NaTe, Ag_2Te, or Sb_2Te_3 in PbTe are used for x_B^α. The heat of solution for NaTe in PbTe is calculated as equal to 26^{+19}_{-11} kJ mol^{-1}, where the error bar corresponds to the error range for the solubility at 240 °C. This value is comparable to 22 ± 1 kJ mol^{-1} for Sb_2Te_3 or 42 ± 11 kJ mol^{-1} for Ag_2Te. This means that the dissolution of NaTe in PbTe is energetically unfavorable in a similar degree to that of Sb_2Te_3 or Ag_2Te. Both Ag_2Te (ref. 20) and Sb_2Te_3 (ref. 38) precipitates form in the nanoscale size in PbTe matrices. In light of the heats of solution in PbTe matrices, the driving force for nucleation is increased considerably by decreasing the temperature according to eqn (4) and the large number of defects in the cast material provides heterogeneous nucleation sites for precipitation. This is highly desirable for forming nano-precipitates. Therefore, it is expected that NaTe precipitates on the nanoscale, similar to Ag_2Te and Sb_2Te_3 through solid state precipitation. This evidently describes the nature of the sodium-rich nano-precipitates observed in a previous study.[14] The observed nano-precipitates

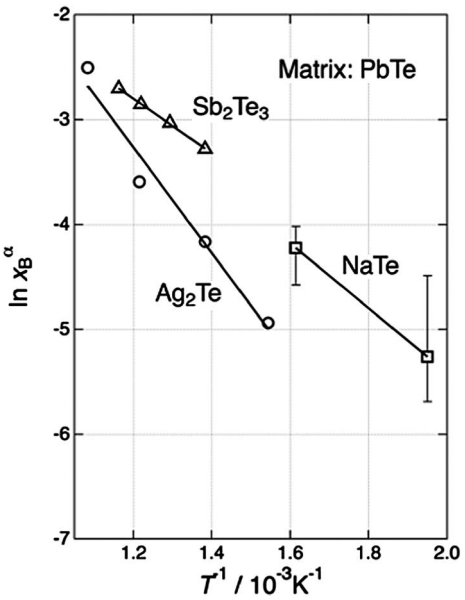

Fig. 5 Temperature dependence of the solubility of NaTe shown together with those of Ag_2Te (ref. 28) and Sb_2Te_3.[29] The solubility of Ag_2Te is corrected taking into account the effect of mutual solubilities.[30]

in the PbTe matrix are thin NaTe precipitates that formed due to the significantly decreased sodium solubility at temperatures less than 320 °C. These thin solid state nano-precipitates are embedded in the PbTe matrix and it is anticipated that they dissolve in the matrix up to the solubility limit when the temperature is increased. The dissolved sodium should then contribute to the electronic properties of PbTe.

Conclusions

In summary, we have measured the maximum solubility of sodium telluride in lead telluride to be 1.4 ± 0.3 mol% at 350 °C. We have shown that the addition of sodium to PbTe beyond this solubility limit results in the formation of a sodium-rich liquid phase at temperatures above 360 °C at grain boundaries, which may affect the mechanical properties of the alloy when cooled. On reducing the temperature below the maximum solubility temperature, solid sodium telluride precipitates in the PbTe matrix. We believe that the nano-precipitates which were observed in previous studies are solid sodium telluride which precipitates from the Na saturated lead telluride during cooling to room temperature as the solubility decreases with temperature. Furthermore, we expect that these nano-precipitates will be re-dissolved in the matrix by heating during application at high temperatures such as in measurements of high temperature thermoelectric properties.

Acknowledgements

This work is supported by the BaoSteel Australia R&D Centre, the Department of Education, Science and Technology (DEST) of Australia, ARC Discovery Early Career Award DE130100310 and the NASA Jet Propulsion Laboratory.

Notes and references

1 E. M. Levin, B. A. Cook, J. L. Harringa, S. L. Bud'ko, R. Venkatasubramanian and K. Schmidt-Rohr, *Adv. Funct. Mater.*, 2011, **21**, 441.
2 L. E. Bell, *Science*, 2008, **321**, 1457.
3 Y. Pei, X. Shi, A. LaLonde, H. Wang, L. Chen and G. J. Snyder, *Nature*, 2011, **473**, 66.
4 K. Biswas, J. He, Q. Zhang, G. Wang, C. Uher, V. P. Dravid and M. G. Kanatzidis, *Nat. Chem.*, 2011, **3**, 160.
5 X. Shi, J. Yang, J. R. Salvador, M. Chi, J. Y. Cho, H. Wang, S. Bai, J. Yang, W. Zhang and L. Chen, *J. Am. Chem. Soc.*, 2011, **133**, 7837.
6 X. Shi, J. Yang, S. Bai, J. Yang, H. Wang, M. Chi, J. R. Salvador, W. Zhang, L. Chen and W. Wong-Ng, *Adv. Funct. Mater.*, 2010, **20**, 755.
7 J. P. Heremans, V. Jovovic, E. S. Toberer, A. Saramat, K. Kurosaki, A. Charoenphakdee, S. Yamanaka and G. J. Snyder, *Science*, 2008, **321**, 554.
8 R. F. Brebrick and E. Gubner, *J. Chem. Phys.*, 1962, **36**, 1283.
9 Y. Pei, A. LaLonde, S. Iwanaga and G. J. Snyder, *Energy Environ. Sci.*, 2011, **4**, 2085.
10 A. J. Crocker, *J. Phys. Chem. Solids*, 1967, **28**, 1903.
11 Q. Zhang, F. Cao, W. Liu, K. Lukas, B. Yu, S. Chen, C. Opeil, D. Broido, G. Chen and Z. Ren, *J. Am. Chem. Soc.*, 2012, **134**, 10031.
12 J. Androulakis, I. Todorov, D.-Y. Chung, S. Ballikaya, G. Wang, C. Uher and M. Kanatzidis, *Phys. Rev. B: Condens. Matter*, 2010, **82**, 115209.
13 Y. Pei, A. F. May and G. J. Snyder, *Adv. Energy Mater.*, 2011, **1**, 291.
14 J. He, J. Androulakis, M. G. Kanatzidis and V. P. Dravid, *Nano Lett.*, 2012, **12**, 343.
15 S. N. Girard, J. He, X. Zhou, D. P. Shoemaker, C. M. Jaworski, C. Uher, V. P. Dravid, J. P. Heremans and M. G. Kanatzidis, *J. Am. Chem. Soc.*, 2011, **133**, 16588.
16 A. J. Crocker and L. M. Rogers, *Br. J. Appl. Phys.*, 1967, **18**, 563.
17 D. J. Singh, *Phys. Rev. B: Condens. Matter*, 2010, **81**, 195217.
18 V. K. Finogenova, A. M. Klimakov, B. A. Popovkin and A. V. Novoselova, *Inorg. Mater.*, 1971, **7**, 1662.
19 I. Blum, D. Isheim, D. Seidman, J. He, J. Androulakis, K. Biswas, V. Dravid and M. Kanatzidis, *J. Electron. Mater.*, 2012, **41**, 1583.
20 Y. Pei, J. Lensch-Falk, E. S. Toberer, D. L. Medlin and G. J. Snyder, *Adv. Funct. Mater.*, 2011, **21**, 241.
21 V. G. Vanyarkho, V. P. Zlomanov and A. V. Novoselova, *Inorg. Mater.*, 1970, **6**, 1534.
22 K. A. Borup, E. S. Toberer, L. D. Zoltan, G. Nakatsukasa, M. Errico, J.-P. Fleurial, B. B. Iversen and G. J. Snyder, *Rev. Sci. Instrum.*, 2012, **83**, 123902.
23 P. F. P. Poudeu, J. D'Angelo, A. D. Downey, J. L. Short, T. P. Hogan and M. G. Kanatzidis, *Angew. Chem., Int. Ed.*, 2006, **45**, 3835.
24 A. J. Crocker and L. M. Rogers, *J. Phys. Colloq.*, 1968, **29**, 129.
25 Y. I. Ravich, B. A. Efimova and I. A. Smirnov, *Semiconducting Lead Chalcogenides*, Plenum Press, New York, 1970.
26 R. Fritts, *Thermoelectric Materials and Devices*, Reinhold Pub. Corp., New York, 1960.
27 A. J. Crocker and B. F. Dorning, *J. Phys. Chem. Solids*, 1968, **29**, 155.
28 K. Bergum, T. Ikeda and G. J. Snyder, *J. Solid State Chem.*, 2011, **184**, 2543.
29 T. Ikeda, V. A. Ravi and G. J. Snyder, *Acta Mater.*, 2009, **57**, 666.
30 J. F. Freedman and A. S. Nowick, *Acta Metall.*, 1958, **6**, 176–183.
31 R. S. Allgaier, *Phys. Rev.*, 1960, **119**, 554.
32 U. Mizutani, *Hume-Rothery Rules for Structurally Complex Alloy Phases*, Taylor & Francis, US, 2010.
33 R. Shannon, *Acta Crystallogr., Sect. A: Cryst. Phys., Diffr., Theor. Gen. Crystallogr.*, 1976, **32**, 751.
34 R. T. Sanderson, *Chemical Bonds and Bond Energy*, Academic Press, New York, 1971.
35 P. Böttcher and R. Keller, *J. Less Common Met.*, 1985, **109**, 311.
36 K. C. Russell, *Adv. Colloid Interface Sci.*, 1980, **13**, 205–318.
37 R. A. Swalin, *Thermodynamics of Solids*, John Wiley & Sons, Inc., New York, 1962.
38 T. Ikeda, N. J. Marolf, K. Bergum, M. B. Toussaint, N. A. Heinz, V. A. Ravi and G. Jeffrey Snyder, *Acta Mater.*, 2011, **59**, 2679.

